A multi-element detector system for intelligent imaging: I-ImaS

Griffiths, J.A.; Metaxas, M.G.; Royle, G.J.; Venanzi, C.; Esbrand, C.; van der Stelt, P.F.; Verheij, H.G.C.; Li, G.; Turchetta, R.; Fant, A.; Gasiorek, P.; Theodoridis, S.; Georgiou, H.; Cavouras, D.; Hall, G.; Noy, M.; Jones, J.; Leaver, J.; Machin, D.; Greenwood, S.; Khaleeq, M.; Schulerud, H.; Østby, J.M.; Triantis, F.; Asimidis, A.; Bolanakis, D.; Manthos, N.; Longo, R.; Bergamaschi, A.; Speller, R.D.

DOI
10.1109/NSSMIC.2006.354430

Publication date
2006

Document Version
Final published version

Published in
IEEE Nuclear Science Symposium Conference Record, 2006. - Vol. 4

A Multi-Element Detector System for Intelligent Imaging: I-ImaS

Jennifer A. Griffiths, *Member, IEEE*, Marinos G. Metaxas, Gary J. Royle, Cristian Venanzi, Colin Esbrand, Paul F. van der Stelt, Hans Verheij, Gang Li, Renato Turchetta, Andrea Fant, Przemyslaw Gasiorek, Sergios Theodoridis, Harris Georgiou, Dionissis Cavouras, Geoff Hall, Matthew Noy, John Jones, James Leaver, Davy Machin, S Greenwood, M Khaleeq, Helene Schulerud, Joar M. Østby, Frixos Triantis, Asimakis Asimidis, Dimos Bolanakis, Nikos Manthos, Renata Longo, Anna Bergamaschi and Robert D. Speller

***Abstract*–I-ImaS is a European project aiming to produce new, intelligent x-ray imaging systems using novel APS sensors to create optimal diagnostic images. Initial systems concentrate on mammography and encephalography. Later development will yield systems for other types of radiography such as industrial QA and homeland security.**

The I-ImaS system intelligence, due to APS technology and FPGAs, allows real-time analysis of data during image acquisition, giving the capability to build a truly adaptive imaging system with the potential to create images with maximum diagnostic information within given dose constraints.

A companion paper deals with the DAQ system and preliminary characterization. This paper considers the laboratory x-ray characterization of the detector elements of the I-ImaS system. The characterization of the sensors when tiled to form a strip detector will be discussed, along with the appropriate correction techniques formulated to take into account the misalignments between individual sensors within the array.

Preliminary results show that the detectors have sufficient performance to be used successfully in the initial mammographic and encephalographic I-ImaS systems under construction and this paper will further discuss the testing of these systems and the iterative processes used for intelligence upgrade in order to obtain the optimal algorithms and settings.

Manuscript received November 15, 2006. This work is funded under European Commission Priority 3: Nano-technologies and nano-sciences, knowledge-based multi-functional materials and new production processes and devices under Contract No. NMP-2-CT-2003-505593.

J. A. Griffiths is with the Department of Medical Physics & Bioengineering, University College London, U.K. (telephone: +44 20 7679 0259, e-mail: j.griffiths@medphys.ucl.ac.uk).

M. G. Metaxas, G. J. Royle, C. Esbrand and R. D. Speller are with the Department of Medical Physics & Bioengineering, University College London, U.K.

C. Venanzi was with the Department of Physics, University of Trieste. He is now with the Department of Medical Physics & Bioengineering, University College London, U.K.

P. F. van der Stelt, G. Li and H. Verheij are with the Academic Centre for Dentistry, Vrije Universiteit & University of Amsterdam, The Netherlands.

R. Turchetta, A. Fant and P. Gasiorek are with the Rutherford Appleton Laboratory, CCLRC, Oxfordshire, U.K.

S. Theodoridis and H. Georgiou are with the Department of Informatics & Telecommunications, University of Athens, Greece.

D. Cavouras is with the Medical Image and Signal Processing Laboratory, Department of Medical Instrument Technology, Technological Education Institution of Athens, Greece.

G. Hall, M. Noy, J. Jones, J. Leaver, D. Machin, S. Greenwood and M. Khaleeq are with the High Energy Physics Group, Department of Physics, Imperial College, London, U.K.

J. M. Østby and H. Schulerud are with the Division of Electronics and Cybernetics, SINTEF, Oslo, Norway.

F. Triantis, A. Asimidis, D. Bolanakis and N. Manthos are with the Department of Physics, University of Ioannina, Greece.

R. Longo and A. Bergamaschi are with the Department of Physics, University of Trieste, Italy.

I. Introduction

I-IMAS (Intelligent Imaging Sensors) is an EU FP6 funded project aiming to produce new, intelligent, specialised x-ray imaging systems utilizing novel Monolithic Active Pixel Sensors (MAPS) to create optimal diagnostic images. MAPS technology allows on-chip processing, leading to the potential to provide real-time analysis of data during image acquisition which can be used as an input into a real-time exposure modulation feedback control. Intelligent imaging systems are initially being constructed for mammography and dental encephalography; however the aim is that future development will lead to systems tailored to other types of radiography, such as industrial quality assessment and homeland security.

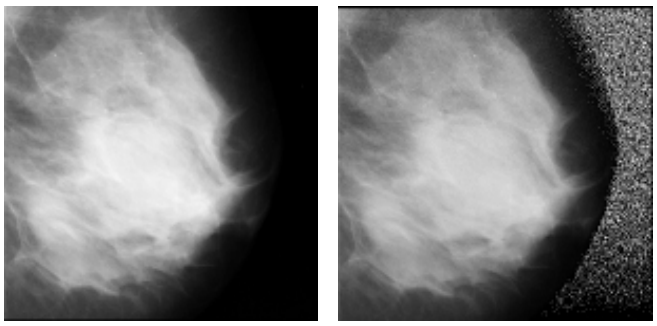

Fig. 1. A model of the I-ImaS principle yielded an image (right), which has the same diagnostic features as a conventional mammographic image (left), but uses 20% less dose.

Radiography systems currently use Automatic Exposure Control (AEC) mechanisms [1-3] to optimise the exposure used to form an image of an object. AEC is done either by inputting parameters such as the object's weight or size or by using a pre-scan – a low dose image of the object which identifies the levels of attenuation present. The image acquisition parameters are then set globally based on data for the entire image such that an optimised image is formed during exposure. These parameters are set once during the entire acquisition process and are constant across the entire image. The I-ImaS system aims to modulate the exposure parameters in real-time across an image, thus optimising them

for individual regions of an object. A preliminary model of this concept based on mammography yielded an image with the same diagnostic quality as a conventional image (Fig. 1), as confirmed by radiologists, but the dose used to form the image was 20% less than that for a conventional image.

II. I-ImaS System Overview

The I-ImaS system (Fig.2) is able to modify image exposure parameters in real-time across an image as it is being acquired, thus optimizing the exposure for individual regions within the image.

A step-and-shoot dual line-scan approach is used; the first line of sensors provides a base image and statistical measures which are processed by FPGAs positioned on the sensor DAQ board [4] to produce feedback parameters for the exposure control system. This system consists of an array of step-wedge filters, allowing real-time modulation of the x-ray beam incident on the second set of sensors in order to obtain an optimal image.

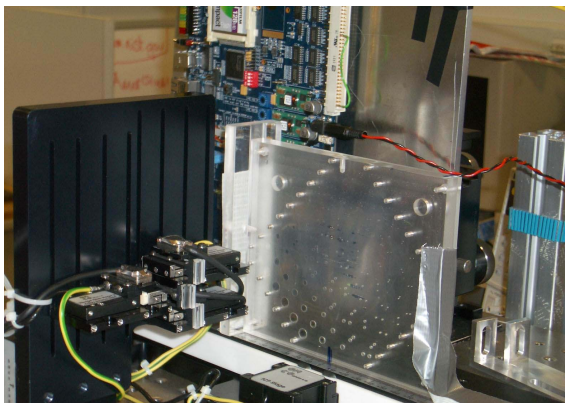

Fig. 2. Photograph of the I-ImaS system working in a laboratory environment. The photograph shows the system imaging a Perspex Contrast Detail phantom. The detector and DAQ are behind the phantom. The dynamic wedge-filters can be seen in front of the phantom.

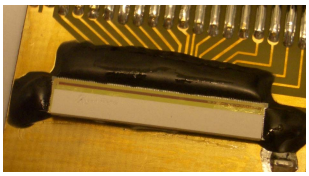

Fig. 3. Photograph of a single I-ImaS sensor with a scintillator in place. The scintillator is coated in white epoxy on five sides in order to maximize light transfer to the sensor.

III. Detector Design Considerations

The sensors, which have been designed specifically for use in this system, are 1.5D Monolithic Active Pixel Sensors with an active imaging area of 32 x 512 pixels, each 32 µm x 32 µm, read out through 16 parallel ADCs. In order to produce a detector suitable for a line-scan imaging approach, the sensors are tiled into a linear array. The sensors' x-ray sensitivity is increased by coupling to scintillators (Fig.3). These were chosen based on empirical and Monte Carlo modeling, experimental work and market availability.

A. Modeling of Scintillators

Empirical modeling of a range of scintillator materials was carried out in order to create a short-list of suitable scintillators for use with the I-ImaS sensors. This modeling aimed to find the best match of scintillator output spectrum to sensor input response. Fig. 4 shows the output spectra for four scintillators compared with the input response of the 6.5 µm silicon technology used for the I-ImaS sensors. This work showed that $Gd_2O_2S(Eu)$ and CsI(Tl) would be the most suitable commercially available scintillators to use with the sensors.

Monte Carlo modeling was then used to further analyse the short-list created by the empirical modeling. This work followed two routes: the first was the use of a ray-tracing model [5] which analysed the light spread in various scintillator structures emanating from a single point of x-ray interaction, indicating the ultimate available spatial resolution of the scintillator. The second route used EGS4 to simulate the attenuation of x-rays produced by mammographic and dental x-ray sources and a monochromatic synchrotron source when incident on various thicknesses of scintillator, thus giving the scintillator efficiency. Using this model, the expected absorption efficiency of 100 µm of CsI(Tl) is 82% for a Mo filtered Mo target (mammographic) x-ray source operating at 40 kVp, and is 52% for an Al filtered W target (dental) source operating at 70 kVp. The mean light yield of CsI(Tl) is 52 light photons per keV of absorbed x-ray energy.

TABLE I
DESCRIPTION OF CSI(TL) SCINTILLATORS USED IN THE EXPERIMENTAL WORK

	Scintillator Type	FOP Thickness (mm)
#1	Unstructured	0
#2	Structured	1
#3	Structured	3

B. Experimental Analysis of Scintillators

The modeling reduced the scintillator choice to the three versions of 100 µm thick CsI(Tl) listed in Table 1. Two experimental protocols were then carried out; one to assess the spatial resolution variation between unstructured and structured scintillators and the other to assess the effect of using a Fiber Optic Plate (FOP) in conjunction with the scintillator.

The experiments to assess the FOP requirement were carried out by coupling the scintillators to a CCD using Cargille Optical Gel 0608 (Cargille Laboratories, Cedar Grove, NJ). The CCD was then placed in front of a mammographic x-ray unit. These experiments highlighted the importance of the presence of a FOP in order to minimize direct x-ray hits in the sensor. However, an FOP will act to degrade the signal observed by the system. This degradation was assessed by measuring the DQE of the CCD system when using scintillators #2 and #3, which are identical except for the FOP on #3 being 2 mm thicker than that found on #2. Fig. 4 shows these results. The DQE falls to 10% at 14 line pairs per millimeter when using the 1 mm thick FOP and at 7 line pairs per millimeter when using the 3 mm thick FOP. This

indicates that, at mammographic energies, the spatial resolution and overall efficiency of the system is significantly degraded by the use of a thicker FOP. Therefore, the 1 mm FOP is preferable.

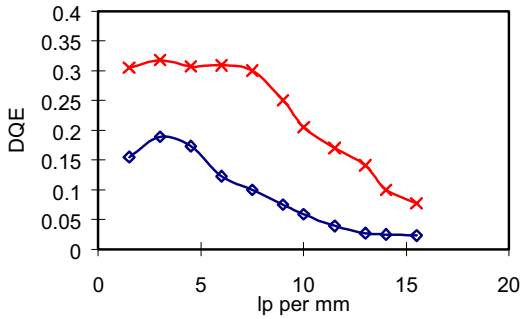

Fig. 4. DQE for scintillators #2 (red crosses) and #3 (blue diamonds) when coupled to a CCD using Cargille Optical Gel 0608. The DQE falls to 10% at 14 lp mm^{-1} for the 1 mm thick FOP (#2) and at 7 lp mm^{-1} for the 3 mm thick FOP (#3).

The variation of spatial resolution with scintillator structure was assessed by coupling scintillators #1 (unstructured, no FOP) and #2 (structured, 1mm FOP) to the I-ImaS sensor using 0.3 µl of Norland Index Matching Liquid 65 (Norland Products, Cranbury, NJ). Characterization of this sensor had previously been carried out using optical wavelengths and x-rays on the naked sensor [4].

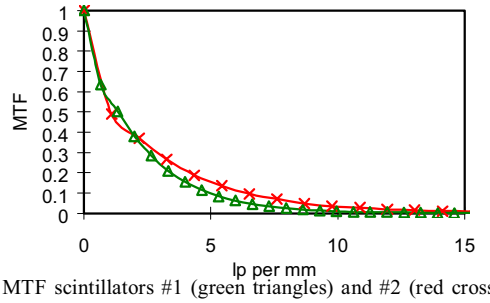

Fig. 5. MTF scintillators #1 (green triangles) and #2 (red crosses) when coupled to an I-ImaS sensor using Norland Index Matching Liquid 65. The MTF drops to 10% at approximately 5 lp mm^{-1} for the unstructured scintillator (#1) and at 6 lp mm^{-1} for the structured scintillator (#2).

The coupled sensor was placed in front of a tungsten target x-ray unit operating a 40 kVp and the MTF of the two scintillators assessed (Fig. 5). The MTF falls to 10% at approximately 5 line pairs per millimeter for the unstructured scintillator (#1) and at 6 line pairs per millimeter for the structured scintillator (#2), giving associated spatial resolutions of 100 µm and 83 µm respectively. The value of spatial resolution achieved using #1 can also be considered to be a 'best case' as, unlike #2, it does not have an FOP which, as previously seen, would act to further degrade the resolution.

These results indicate that the most suitable of the three scintillator samples investigated is #2 as it offers the best compromise between spatial resolution, reduction of direct hits in the sensor and detection efficiency.

IV. Image Formation

The I-ImaS sensors have an imaging area approximately 1 mm x 16 mm in size. Therefore, tiling of the sensors is necessary in order to form an imaging area suitable for a line-scan medical imaging system. The tiling must be carried out such that there is an overlap between the sensors to ensure that acquired images cover the entire area to be imaged (Fig.6). An overlap will also be required in the direction of the detector scan, implying that the step size chosen for the step-and-shoot protocol should be less than an entire sensor width.

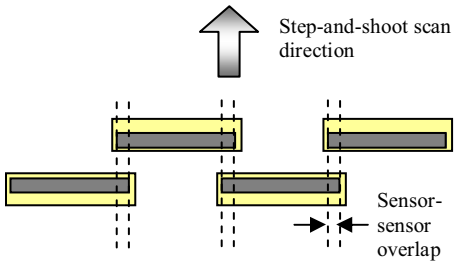

Fig. 6. Schematic diagram showing the overlapped sensor layout used to form a line-scan detector. The active imaging area of each sensor is shaded.

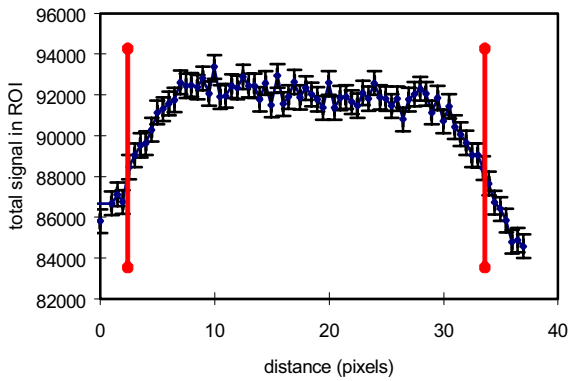

Fig. 7. Plot of the total signal in a 5 x 5 pixel ROI as the detector is moved across a pin-hole in half-pixel steps. The edges of the imaging area of the sensor are marked by the red lines. This indicates that the central 26 pixels can be considered to give a uniform response.

An investigation was carried out to assess the uniformity of the detector across its short (32 pixel) dimension. The detector was placed on a high precision translation stage and moved in half-pixel (16 µm) steps across a pencil beam of x-rays defined by a 20 µm radius pin-hole collimator. At each translation point, an image of the pin-hole was acquired; this was then corrected for fixed pattern noise and the pixel containing the maximum signal identified. This pixel was considered to be the centre of the pin-hole image. The total signal in a 5 pixel x 5 pixel ROI centered on this pixel was then recorded for each image.

Fig. 7 shows the total signal in the ROI against the distance traveled by the detector from an arbitrary datum. The bounds of the detector have been marked on the figure. The plot shows that within errors, the central 26 pixels on the sensor can be considered to give a uniform response. This means that a three pixel overlap is required between the step-and-shoot

translation positions in order to ensure a uniformly acquired image achieving maximum system DQE.

The ideal positioning of the overlapped sensors within the linear detector array would be such that their axes are parallel (i.e. the sensors are 'square' to each other) and the sensor-sensor overlap is an integral multiple of the pixel pitch. Mechanical limitations when placing the sensors in the array mean that there will be some deviation from this ideal situation. This deviation must be corrected by post-processing in order to create diagnostically useful images. Nevertheless, despite the necessity of this correction, manipulation of the images in order to perform the correction will cause degradation of the system MTF.

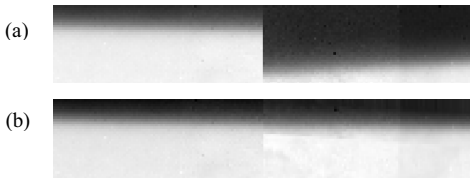

Fig. 8. Images of an edge placed across two I-ImaS sensors before (a) and after (b) a simple misalignment correction has been applied.

In order to assess the effects on the system MTF of correcting the image, a metal edge was placed across two misaligned sensors and an image obtained (Fig. 8(a)). The image was then corrected for the misalignment (Fig 8(b)) and the MTF obtained for both the uncorrected and corrected images (Fig. 9). A significant discontinuity can be observed in Fig. 8(a); this indicates gross linear and rotational misalignments between the two sensors.

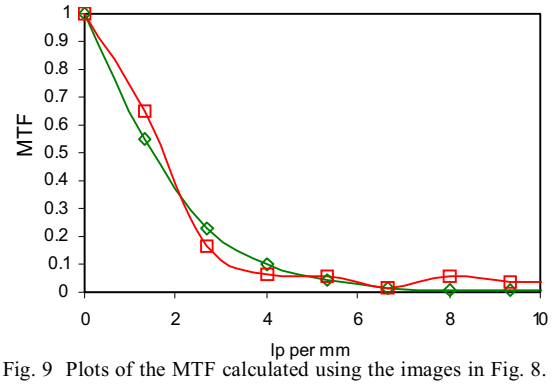

Fig. 9 Plots of the MTF calculated using the images in Fig. 8. The green diamonds indicate the use of the data from the two sensors shown in Fig. 8(a); the red squares use data taken from Fig. 8(b) – the corrected two sensor image. The MTF for the corrected image shows oscillations due to the interpolation procedures used in the rotational correction.

In order to obtain the image in Fig. 8(b), the data on the right hand side of Fig 8(a) was manipulated in two steps to create a single edge across the image. Firstly, a linear translation was performed based on the data in the pixel columns immediately either side of the discontinuity; a profile was obtained for each column and the pixel containing the median grey level value was found for each. The data on the right-hand side of Fig. 8(a) was then moved linearly such that the median pixel to the right of the discontinuity had the same vertical co-ordinate as the median pixel to the left of the discontinuity. The second stage of the manipulation rotated the data to the right of the discontinuity around the median pixel point such that a straight edge was obtained across the image. The rotation algorithm used bilinear interpolation in order to obtain the new pixel grey level values. For this particular data set, the linear translation was 17 pixels, equating to a distance of 544 μm and the required rotation angle was found to be 3.5°. This rotational displacement is considered to be at the bounds of poor sensor placement for this system, thus giving a near worst-case scenario.

Pre-sampled MTFs were obtained for both images in Fig. 8. Two MTFs were obtained for the top image; one for each sensor. These were then averaged to give and average MTF for uncorrected individual sensor data. This is indicated by the green line marked with diamonds in Fig. 9. A single MTF curve using all the data in Fig. 8(b) was obtained for analysis of the system MTF after correction of the data has occurred. This is indicated by the red line marked with squares in Fig. 9. This plot shows considerable oscillation, which we consider to be due to the current rotation correction technique using bilinear interpolation. This indicates that further work is necessary to provide a quality data manipulation algorithm with the ability to minimize the loss of data in the images.

V. A Functional Imaging System

The I-ImaS imaging system will acquire images using a linear tiled detector array (Fig. 6) operating in a step-and-shoot fashion. The final systems will operate with the object being held still whilst the complete imaging system is scanned across – an essential feature for a scanning medical imaging system. However, the prototype system has been constructed such that the object (e.g. mammographic phantom) being imaged scans through a stationary imaging system. The temporary reversal of the system/object scan mechanism has removed additional mechanical complexity, allowing the focus of the project to move towards optimal image creation, rather than system mechanics.

A pre-prototype I-ImaS system has been used without full intelligence implementation to obtain images of small test objects. Fig. 10 shows an image of a piece of jaw and three teeth, the middle one having small ball-bearing positioning markers attached taken using 70 kVp tungsten x-rays. Gain and dark noise corrections have been applied. The image was formed by scanning the object in the horizontal direction. 56 frames data frames have been stitched together to form the image. These were acquired with a step distance of 26 pixels, equating to the three pixel overlap required by the analysis of the data in Fig. 7. The image indicates the dynamic range of the sensors, showing the ball-bearings, tooth root and structures within the jaw-bone clearly.

These results from the pre-prototype system show that the I-ImaS system is capable of producing good diagnostic quality images. The prototype system, which operates a full 10 sensor long detector array with intelligence driven step-wedge modulation of the x-ray beam quality has now been constructed based on this pre-prototype system and is

currently undergoing acceptance testing and commissioning. Characterization of this system is imminent and results are expected in early 2007. It is hoped that this prototype system will prove to be capable of producing intelligent images containing an increased level of diagnostic information compared to current AEC systems.

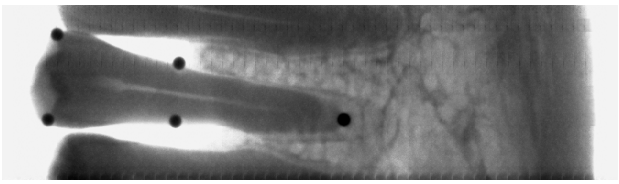

Fig. 10 Image of a piece of jaw and three teeth (one containing ball-bearing positioning markers). The image has been formed by stitching together 56 individual frames from a step-and-shoot acquisition.

REFERENCES

[1] D. Plewes and E. Vogelstein, "A scanning system for chest radiography with regional exposure control: Practical Implementation", *Med. Phys.*, vol. 10, no. 5, pp. 655-663, 1983.

[2] I. A. El-Bakri, A. V. Lakshminarayanan, and M. M. Tesic, "Automatic exposure control for a slot scanning full field digital mammography system", *Med. Phys.*, vol.32, no. 9, pp. 2763-2770, 2005.

[3] F. E. Eraso, J. B. Ludlow, E. Platin, D. Tyndall, and C. Phillips, "Clinical and in vitro film quality comparison of manual and automatic exposure control in panoramic radiography", *Oral Surg. Oral Med. Oral Pathol. Oral Radiol. Endod.*, vol. 87, no. 4, pp. 518-523, 1999.

[4] M. Noy *et al.*, "Adaptive Imaging using the I-ImaS x-ray imaging system", *Proc. IEEE NSS & MIC, 2006*, submitted for publication.

[5] D. Cavouras, Technological Education Institution. Of Athens, Greece, personal communication, 2005.